

Combining IST-Based CFO Compensation and Neural Network-Based Demodulation for Eigenvalue-Modulated Signal

Ken Mishina , Member, IEEE, Takaya Maeda, Daisuke Hisano , Member, IEEE, Yuki Yoshida , Member, IEEE, and Akihiro Maruta , Member, IEEE, Member, OSA

Abstract—Eigenvalue-based communication technologies using inverse scattering transform (IST) have gained attention as a new transmission strategy in optical fiber communications. In recent years, several studies on artificial neural network (ANN)-based equalization and demodulation schemes for eigenvalue-modulated signal have been conducted to enhance the receiver sensitivity. However, in the case of a presence of a carrier frequency offset (CFO) at receiver, the effects of the CFO on ANN receiver of eigenvalue-modulated signal is yet to be reported. In this study, we numerically and experimentally investigated the generalization performances of eigenvalue domain ANN-based demodulator on CFO. Furthermore, we propose to combine an ANN-based demodulator with a CFO compensation method based on IST and a relation between frequency and eigenvalue shifts. The proposed method, based on an appropriate soliton pulse, achieves a high CFO estimation accuracy of submegahertz order even if the CFO reaches ± 2.5 GHz under the noiseless condition. In the presence of noise and a large CFO of 2.5 GHz, the method attains a CFO estimation accuracy below 60 MHz for OSNR = 10 dB with a low pilot pulse rate, such as 0.064%. We show the simulation results obtained after applying the proposed CFO compensation to the ANN demodulator, which is valid for 2.5 GHz CFO and long-haul transmission over 5000 km. Experiments performed in this study demonstrate successful demodulation of an eigenvalue-modulated signal with OSNR penalty < 1 dB in the presence of CFO within 1 GHz at 2.5 Gb/s.

Index Terms—Artificial neural networks, frequency estimation, machine learning, optical fiber communication, optical solitons.

I. INTRODUCTION

OPTICAL eigenvalue communication [1] based on inverse scattering transform (IST) [2] has been recently gained

Manuscript received April 1, 2021; revised June 15, 2021 and September 10, 2021; accepted September 18, 2021. Date of publication September 22, 2021; date of current version December 2, 2021. This work was supported in part by the Grants-in-Aid for Scientific Research under the Japan Society for the Promotion of Science (JSPS) under Grant JP19H02140. (*Corresponding author: Ken Mishina*)

Ken Mishina, Takaya Maeda, Daisuke Hisano, and Akihiro Maruta are with the Graduate School of Engineering, Osaka University, Suita, Osaka 565-0871, Japan (e-mail: mishina@comm.eng.osaka-u.ac.jp; maeda@pn.comm.eng.osaka-u.ac.jp; hisano@comm.eng.osaka-u.ac.jp; maruta@comm.eng.osaka-u.ac.jp).

Yuki Yoshida is with the Graduate School of Engineering, Osaka University, Suita, Osaka 565-0871, Japan, and also with the National Institute of Information and Communications Technology (NICT), Koganei, Tokyo 184-8795, Japan (e-mail: yuki@nict.go.jp).

Color versions of one or more figures in this article are available at <https://doi.org/10.1109/JLT.2021.3114427>.

Digital Object Identifier 10.1109/JLT.2021.3114427

attention because it is unaffected by the Kerr nonlinearity in optical fibers [3]–[24]. Recently, IST has become well-known as the nonlinear Fourier transform (NFT). Propagation of optical pulse is governed by nonlinear Schrödinger equation (NLSE), which can be theoretically solved by IST. Eigenvalues in eigenvalue equations associating with the NLSE are invariant without depending on propagation distance. Although optical waveforms and frequency spectra of optical signal change during propagation in nonlinear dispersive fibers, eigenvalues do not change provided that the NLSE is satisfied.

The concept of eigenvalue communication was proposed by Hasegawa and Nyu in 1993 [1]. Owing to the recent remarkable development of digital coherent technologies, it has become possible to realize the concept of the eigenvalue communication [6], [7]. To increase transmission capacity, various advanced modulation and transmission schemes based on IST have been reported over the past several years, such as M-ary QAM of discrete spectral amplitude or scattering coefficient $b(\zeta_n)$ [8], [9] and on-off encoding of multieigenvalue ζ_n [10], [11]. As high-order multi-level modulations, 64-QAM of spectral amplitude [8] and 16-QAM of $b(\zeta_n)$ [9] have been proposed. A high-capacity transmission using dual-polarization b -modulation with a net data rate of 220-Gb/s and a spectral efficiency (SE) of 4 bits/s/Hz has been achieved in experiment [12]. Furthermore, a 16-ary eigenvalue-modulated signal transmission using an on-off encoding over 3000 km has been experimentally demonstrated [13]–[15].

To improve the received power margin, machine-learning-based demodulation and equalization methods for eigenvalue-modulated signal have been investigated in recent years [13]–[21]. Demodulation methods based on time-domain (TD) artificial neural networks (ANNs) for b -modulation have outperformed the conventional IST-based demodulation method in terms of the bit error rate (BER) performance with a large power margin [16].

The successful demodulation of TD-ANN with a phase recovery has been experimentally demonstrated even in the presence of a carrier frequency offset (CFO) [17]. A regression neural network receiver in TD for QAM of spectral amplitude, which has the robustness to laser phase noise, was also proposed [18]. As an improved approach, a bidirectional long short-term memory gated recurrent neural network equalizer has been proposed and shown to outperform a feed-forward ANN equalizer at a spectral

amplitude of 64-QAM of spectral amplitude [19]. However, these ANN-based receivers have been demonstrated only with a small static CFO ≤ 100 MHz generated by simulation or using acousto-optic modulator in experiment. There has been no study on demonstration and analysis of ANN-based receiver for IST-based transmission in the presence of a large CFO, considering a micro-ITLA laser [22], [23].

For on-off encoding of multieigenvalue, the authors have proposed an eigenvalue domain (ED)-ANN-based demodulation method, which does not require model training for each transmission distance [15]. In this study, we focus on the ED-ANN-based receiver for the on-off encoded signal. In the presence of a CFO at the receiver, CFO in the frequency domain (FD) is converted to an eigenvalue shift in the ED. This eigenvalue shift causes a performance degradation of the ED-ANN demodulator, which requires a detected eigenvalue pattern as the input. In other words, if a large CFO is present, the ED-ANN requires model training for each CFO owing to the eigenvalue shift. Moreover, a detailed analysis of the effects of the CFO on the ED-ANN receiver for eigenvalue-modulated signal is yet to be reported.

In this study, we numerically and experimentally investigate the generalization performances of ED-ANN-based demodulator on CFO. Moreover, we propose to combine an ED-ANN-based demodulator with a CFO compensation method based on IST to emphasize robustness against variation in CFO. As an extension of our previous research [20], [21], we have described the CFO estimation method in detail along with the further investigations of basic characteristics pertaining to the proposed method, such as accuracy of CFO estimation when changing time window size, sampling rate, eigenvalue, and noise effects. By using an appropriate soliton pulse, a high estimation accuracy of submegahertz order is obtained for a CFO reaching ± 2.5 GHz under the noiseless condition. Even in the presence of noise and a large CFO of 2.5 GHz, the proposed CFO estimation achieves an accuracy of CFO estimation below 60 MHz for optical signal-to-noise ratio (OSNR) of 10 dB even with a low pilot pulse rate, such as a pulse rate of only 0.064%. Simulation results obtained in this study demonstrate that the ED-ANN demodulator with the proposed CFO compensation achieves a successful demodulation with almost no OSNR penalty in the presence of CFO within 2.5 GHz. The applicability to long-haul transmission over 5000 km is also demonstrated through the simulation. Furthermore, experiments performed in this study demonstrate successful demodulation of an eigenvalue-modulated signal with OSNR penalty < 1 dB in the presence of CFO within 1 GHz at 2.5 Gb/s.

The remainder of this paper is organized as follows. Section II describes the eigenvalue-modulation method involving on-off encoding and ED-ANN-based demodulation method. Section III describes the proposed CFO estimation method and its application to the CFO compensation on ED-ANN demodulator. Section IV discusses results of the performed numerical simulations. Section V discusses proof-of-concept experiments performed in this study to demonstrate the feasibility of the proposed method. Finally, Section VI lists major conclusions drawn from this study.

II. EIGENVALUE MODULATION AND DEMODULATION

A. Eigenvalue Modulation

Consider a normalized complex-envelope amplitude $u(Z, T)$ of an electrical field propagating along an optical fiber that exhibits anomalous dispersion and nonlinearity. The propagation can be modeled by the following normalized NLSE [25]

$$i \frac{\partial u}{\partial Z} + \frac{1}{2} \frac{\partial^2 u}{\partial T^2} + |u|^2 u = 0, \quad (1)$$

where Z and T are the normalized quantities of propagation distance and time, moving with the averaged group velocity, respectively. Eigenvalue equation associated to (1) is provided by

$$\frac{\partial \psi}{\partial T} = \begin{bmatrix} -i\zeta & iu \\ iu^* & i\zeta \end{bmatrix} \psi, \quad (2)$$

where ζ and $\psi = (\psi_1, \psi_2)^T$ are complex eigenvalue and eigenfunction vector, respectively. Provided $u(T, Z)$ satisfies (1), eigenvalue ζ is invariant with respect to Z .

In this study, an eigenvalue modulation based on on-off encoding was employed. In the eigenvalue modulation, N -soliton solutions that have N eigenvalues are used as input pulse [24]. Fig. 1 depicts the block diagram of modulation and demodulation using an on-off encoding of multi-eigenvalue. The on-off encoding is based on a one-to-one mapping between an N -bit input and the 2^N subsets of eigenvalues. If the value of the bit in the j -th position is 1 (or 0), then j -th eigenvalue is included (or excluded). In this section, we explain an example of $N = 4$. First, the four information bits are encoded to a complex eigenvalue pattern, for example, “1111” and “1001” are assigned to eigenvalue patterns of “ $\zeta = \{0.25 + 0.5i, -0.25 + 0.5i, 0.25 + 0.25i, -0.25 + 0.25i\}$ ” and “ $\zeta = \{-0.25 + 0.5i, 0.25 + 0.25i\}$,” respectively. Thereafter, the encoded eigenvalue pattern is mapped to a pulse using IST. The optical signal generated by IQ modulator is launched into fiber transmission line. That is, N information bits are converted to optical pulse shape, which contains an on-off pattern of the N -tuple of eigenvalues.

At the receiver, the transmitted optical signal is received with a generic coherent receiver to divide the optical signal into IQ components. Thereafter, the IQ signal waveform is divided into each pulse waveform. After the windowing and normalization, an eigenvalue pattern is detected from a received pulse using IST. For eigenvalue detection, we used the Fourier collocation method [5], [7], [27], because a root-search algorithm, such as the Newton-Raphson method, is not suitable for finding the “off” state of the eigenvalue in the on-off encoding. In the Fourier collocation method, the received pulse is converted in the spectrum domain by a Fourier transform. Consequently, eigen functions ψ are expanded in the Fourier series and Eq. (2) is reformulated as an eigenvalue problem in the Fourier space. Finally, the detected eigenvalue pattern is decoded to an information bit sequence.

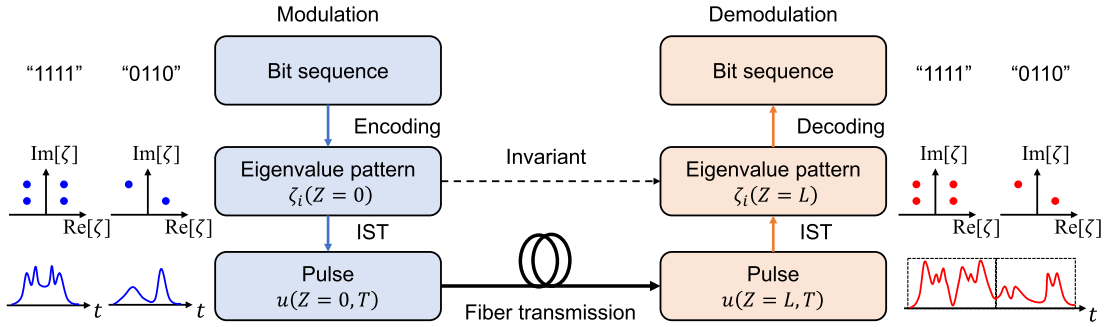


Fig. 1. Block diagram of eigenvalue modulation–demodulation scheme based on on–off encoding of four eigenvalues ($N = 4$).

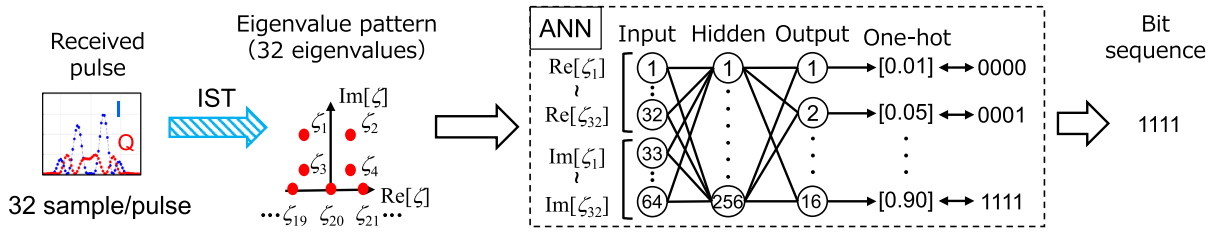


Fig. 2. ED-ANN-based demodulation [15].

B. ED-ANN-Based Demodulation

In the conventional scheme, the detected eigenvalue pattern is decoded via appropriate setting of linear thresholds on the complex eigenvalue plane. However, the authors proposed an ED-ANN-based demodulation method [15], as shown in Fig. 2. In particular, the detected eigenvalues are considered ANN input, and probability factors of bit sequences corresponding to detected eigenvalue patterns are considered ANN output. Fig. 2 depicts the configuration of the ANN-based demodulator for four eigenvalues ($N = 4$). For a sampling rate of 32 sample/pulse, the number of converted eigenvalues, including continuous spectrum near the real axis, equals 32. The number of the input elements comprising 32 real and imaginary parts each of eigenvalues is 64. Before inputting to the ANN, the eigenvalues are sorted in an ascending order for the real part of eigenvalue. The number of output elements equals 16 based on the number of eigenvalue patterns—i.e., $2^4 = 16$. The ED-ANN demodulator outperformed its conventional demodulation with a large power margin owing to high-dimensional nonlinear classification of the ANN. Moreover, it does not require performing model training when considering different transmission distances because eigenvalue patterns are invariant during lossless transmission.

III. CFO COMPENSATION METHOD

1-soliton pulse that has an eigenvalue is considered. The complex eigenvalue ζ is expressed by

$$\zeta = \frac{\kappa + i\eta}{2}, \quad (3)$$

where κ and $\eta (> 0)$ are real numbers. The 1-soliton solution is provided by

$$u(Z, T) = \eta \operatorname{sech}\left\{\eta(T + \kappa Z)\right\} \exp\left(-i\kappa T + i\frac{\eta^2 - \kappa^2}{2}Z\right). \quad (4)$$

where free parameters τ_s and ϕ_s are set to zero [26]. When 1-soliton pulse is received at $Z = L$, the phase of the pulse $u(L, T)$ changes in proportion to $-\kappa T$. From (4), we can interpret that κ and η correspond to the soliton frequency and amplitude (pulse width), respectively. Therefore, a frequency shift at the receiver, namely CFO, appears as a shift of the real part of the detected eigenvalue $\operatorname{Re}[\zeta] = \kappa/2$ in the ED. Regarding the frequency shift, the following relationship between the time domain pulse $u(T)$ and eigenvalue ζ is common,

$$u(T) \exp(-i2\pi FT) \iff \zeta - \pi F, \quad (5)$$

where F represents the normalized frequency.

In the digital coherent receiver, a CFO is caused by the frequency mismatch between the carrier signal and local oscillator (LO). The frequency error of the laser can reach up to ± 2.5 GHz with a micro-ITLA [22], [23]. A large CFO induces a symbol decision error in the conventional and ED-ANN demodulations. Fig. 3 shows a CFO effect on the detected eigenvalue patterns for $N = 4$. In the presence of CFO of over 2 GHz, a large eigenvalue shift across the imaginary axis on the complex eigenvalue plane is observed. Although the ED-ANN demodulator has a great generalization performance on transmission distance, the former approach requires model training for each CFO owing to the above-described eigenvalue shift. Therefore, to emphasize the robustness against variation of CFO, we propose combining a

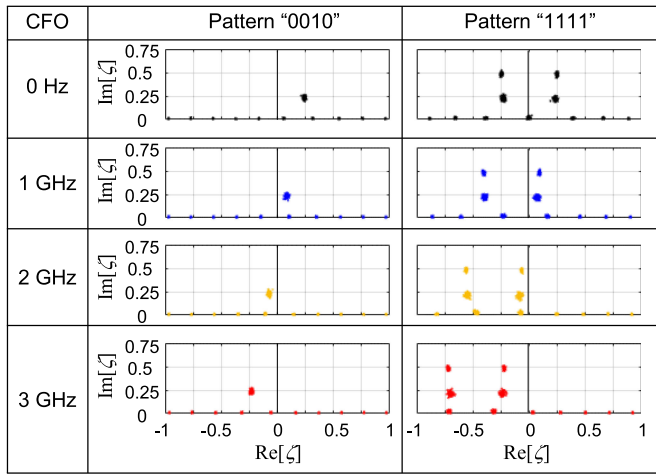


Fig. 3. Effect of CFO on the detected eigenvalue pattern.

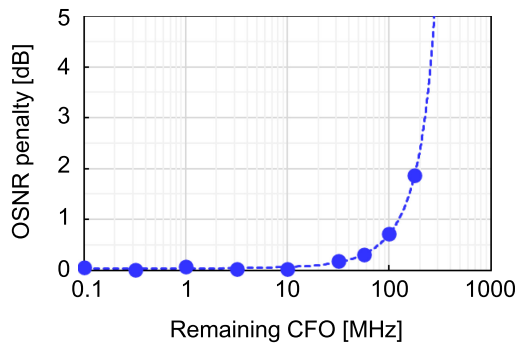


Fig. 4. Variation in OSNR penalty with remaining CFO for eigenvalue modulation based on on-off encoding.

CFO estimation method in the ED with the ED-ANN demodulator. In the eigenvalue modulation based on on-off encoding, the phase of the soliton pulse is not used for the modulation. Therefore, a coarse CFO estimation is sufficient for demodulation, and a fine phase recovery is not required.

Fig. 4 shows the variation in OSNR penalty with remaining CFO for eigenvalue-modulated signal based on on-off encoding. The condition of modulation and ED-ANN demodulation specified in the simulation [15] were adopted. The CFO was set to a fixed value of 1 GHz, and the remaining CFO was adjusted via manual CFO compensation without a CFO estimation in the simulation. The OSNR penalty at the forward error correction (FEC) limit compared with an ideal fine CFO compensation and phase recovery is plotted in Fig. 4. The result indicates the penalty can be kept below 1 dB with a coarse CFO compensation of 100 MHz for the system described in [15].

Phase recovery processing is essential when nonlinear spectral amplitude modulation or b -modulation, including soliton phase modulation [8], [9] is employed. A few studies combining a CFO compensation, phase recovery, and an ANN-based receiver have been reported [17], [18]. In [17], a two-stage iterative carrier recovery with a ANN-based phase estimator and a moving average filter was proposed. Although they inserted

a coarse CFO estimation before the phase recovery, the CFO generated by AOM was static and not estimated. In [18], CFO estimation and carrier phase estimation were performed by a blind phase search algorithm under a fixed condition with a CFO of 100 MHz and linewidth of 100 kHz. The performance for a large CFO assuming micro-ITLA is still open to discussion.

For a general QAM system (not IST-based), a coarse CFO estimation and compensation are performed before phase recovery in typical feed-forward digital signal processing methods. Several studies have been reported on CFO estimation methods [28]–[30], such as an algorithm using a periodogram in the FD for general QAM systems [30]. However, such a periodogram-based approach requires a large number of samples to achieve high accuracy CFO estimation.

Recently, IST-based CFO estimation methods have been reported [21], [31]. In related work [31], CFO is estimated in the ED and compensated in the scattering coefficient $b(\zeta)$ domain for b -modulation. It is expected that the CFO estimation in the ED is more accurate than that in the linear FD, particularly for CFO below half of baud rate. In this work, we estimate CFO in the ED and compensate it in the TD for an on-off encoded signal to obtain the same detected eigenvalue patterns without depending on CFO value. The IST-based CFO estimation in the ED has the potential to achieve high accuracy with a small number of samples because the IST-based eigenvalue detection includes the extraction of the soliton component, namely soliton fitting. Furthermore, the algorithm has the potential to be valid for different transmission distances because the eigenvalue is invariant during lossless transmission.

Fig. 5 depicts an overview of the proposed CFO estimation and compensation methods. CFO caused at the receiver corresponds to the shift of real part of the detected eigenvalue in Eq. (5). If the transmitted eigenvalue ζ_t is known, then the CFO can be estimated by comparing ζ_t and the detected eigenvalue ζ_r at the receiver that includes CFO effect. The estimated CFO \hat{f}_{offset} is expressed by

$$\hat{f}_{\text{offset}} = \frac{\text{Re}[\zeta_t] - \text{Re}[\zeta_r]}{\pi t_0}, \quad (6)$$

where t_0 is the base time satisfying $T = t/t_0$ and t is the actual time. When the speed of the CFO change is significantly slower than the baud rate, the CFO can be compensated using the estimated CFO from periodic pilot soliton pulses as a preamble, as shown in Fig. 5(b). In this method, we consider a fundamental soliton pulse with one eigenvalue as a pilot pulse. Therefore, ζ_t and ζ_r are scalar. At the receiver, ζ_r can be selected by extracting an eigenvalue that has the maximum imaginary part among all the detected eigenvalues. We apply this concept to an ED-ANN demodulator. The ED-ANN demodulator is pre-trained using a random eigenvalue-modulated signal and receiver that has a small CFO effect. Here, the detected eigenvalue ζ_{train} of the same pattern as pilot soliton pulse is stored in the memory. When the eigenvalue-modulated signal is received at an arbitrary receiver that has an arbitrary CFO value, the CFO can be estimated

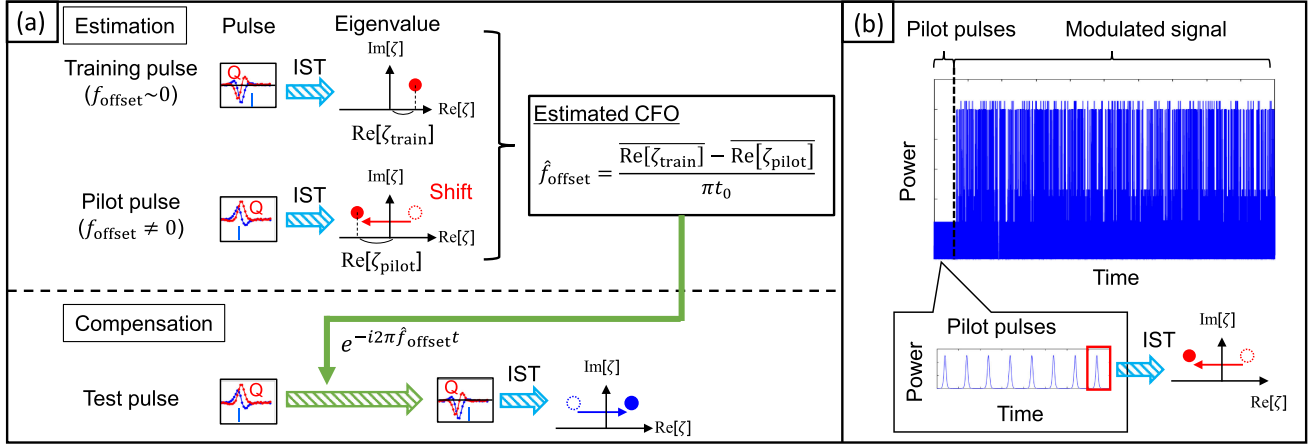


Fig. 5. Proposed CFO compensation method: (a) CFO estimation and compensation, (b) insertion of periodic pilot soliton pulses.

from the detected eigenvalue ζ_{pilot} of the pilot pulse,

$$\hat{f}_{\text{offset}} = \frac{\overline{\text{Re}[\zeta_{\text{train}}]} - \overline{\text{Re}[\zeta_{\text{pilot}}]}}{\pi t_0}. \quad (7)$$

The CFO of the received signal is compensated by multiplying $\exp(-i2\pi\hat{f}_{\text{offset}}t)$ in the time domain. By detecting eigenvalue from the CFO-compensated signal, the eigenvalue pattern without shift owing to CFO can be obtained. Therefore, the ED-ANN does not require training for each CFO using the compensated eigenvalue pattern as an input to the ANN.

IV. NUMERICAL SIMULATIONS

This section describes numerical simulations, combining the proposed CFO compensation method with an ED-ANN demodulator to demonstrate the demodulation of the eigenvalue-modulated signal. First, we analyze the CFO estimation accuracy of the proposed CFO estimation method in the ED. Thereafter, we show the demodulation results with and without the CFO compensation.

A. Accuracy of CFO Estimation

1) *Simulation Model:* We constructed a simple simulation to investigate the accuracy of the CFO estimation method in the ED, as shown in Fig. 6. The fundamental soliton with an eigenvalue was employed to estimate CFO. The transmitted eigenvalue ζ_t was stored in the memory as a known value. The eigenvalue pattern was detected by the Fourier collocation method [5], [7], [27] from the received pulse at the receiver. The received eigenvalue ζ_r for the CFO estimation was obtained by extracting an eigenvalue that had the maximum imaginary part. Then, the CFO was estimated based on Eq. (6). We evaluated the accuracy by changing the following parameters: the eigenvalue, time window size W , and sampling rate R_s . The base time t_0 was set to 50 ps. The relationships between normalized and actual parameters for $t_0 = 50$ ps are summarized in Table I. The number of pulses N_p was changed only when white Gaussian noise and laser phase noise were added to the eigenvalue-modulated signal in the time domain.

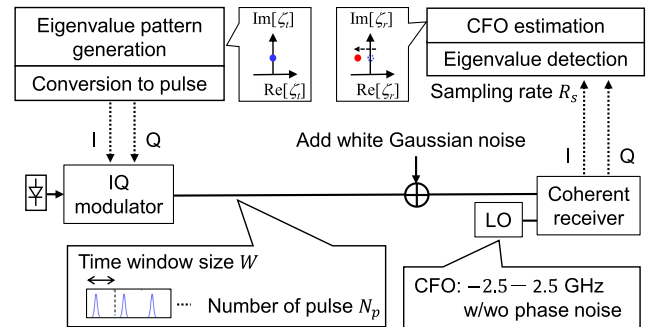


Fig. 6. Simulation model to investigate the estimation accuracy.

TABLE I
RELATIONSHIPS BETWEEN NORMALIZED AND ACTUAL PARAMETERS ($t_0 = 50$)

Time window size W

Normalized	4	8	16	32	64	128	256	512
Actual (ns)	0.2	0.4	0.8	1.6	3.2	6.4	12.8	25.6

Sampling rate R_s

Normalized	1/8	1/4	1/2	1	2	4	8	16
Actual (GSa/s)	2.5	5	10	20	40	80	160	320

In this study, we compare the IST-based CFO estimation method in the ED with fast Fourier transform (FFT)-based method in the FD, which is similar to the periodogram method [30]. In the FFT-based method, the CFO is estimated by calculating the difference in peak frequencies between the transmitted pilot pulse (known) and received pilot pulse. The frequency spectrum is calculated by FFT; hence, the frequency estimation accuracy depends on the FFT window size, namely the time window size W .

2) *Simulation Results Without Noise:* First, we describe the results without noise loading to discuss the fundamental characteristics of the ideal CFO estimation in the ED. The CFO was estimated from one soliton pulse ($N_p = 1$) on the noiseless condition. Fig. 7 shows the estimation error when changing the CFO and $\text{Im}[\zeta]$ for $W = 64$

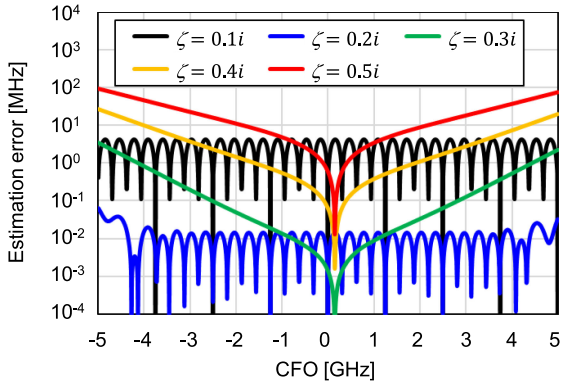


Fig. 7. CFO estimation error varying CFO and imaginary part of eigenvalues.

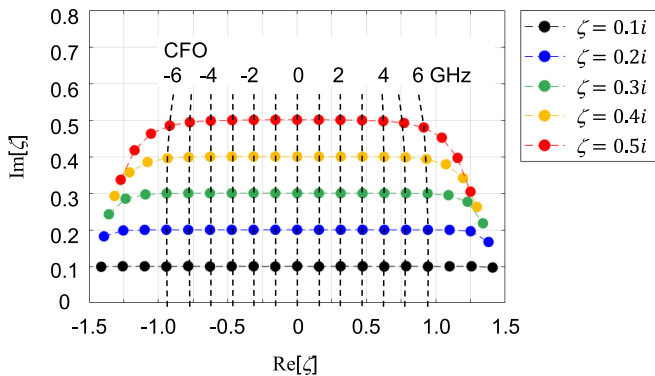


Fig. 8. Detected eigenvalues varying CFO and imaginary part of eigenvalues.

(3.2 ns) and $R_s = 1$ (20 GSa/s). The error of CFO estimation denotes an absolute value of difference in CFO between estimated and real values $|\hat{f}_{\text{offset}} - f_{\text{offset}}|$ (to be the same afterwards).

In the cases of $\zeta = 0.1i$ and $0.2i$, the estimation errors periodically change by the CFO value. This result comes from the eigenvalue detection based on the Fourier collocation method, and the period corresponds to the FFT resolution of 0.3125 GHz ($= 1/W$). In the Fourier collocation method, the eigenvalue pattern is detected by solving the eigenvalue problem in the discrete frequency domain via FFT. The tail of an ideal soliton pulse is distributed between $-\infty$ and $+\infty$ in the time domain. However, the soliton pulse is trimmed in the time domain during the FFT process. In addition, the time window size W limits the resolution in the FD, which also limits the soliton frequency resolution in the ED. Therefore, the CFO estimation accuracy is limited by the time window size W for long-tail soliton pulses with $\zeta = 0.1i$ or $0.2i$, and the maximum error appears at the peak of the period.

In contrast, in the cases of eigenvalues $\zeta = 0.3i, 0.4i$, and $0.5i$, the estimation error increases with the CFO. This phenomenon is caused by the eigenvalue shift owing to bandwidth limitation. The spectrum of an ideal soliton pulse is also distributed between $-\infty$ and $+\infty$ in the FD. However, the spectrum is trimmed in the FD during the FFT process. Fig. 8 shows the detected eigenvalue for several eigenvalues and CFO values ($W = 64$ and $R_s = 1$). The eigenvalue detection area is limited, and a large eigenvalue

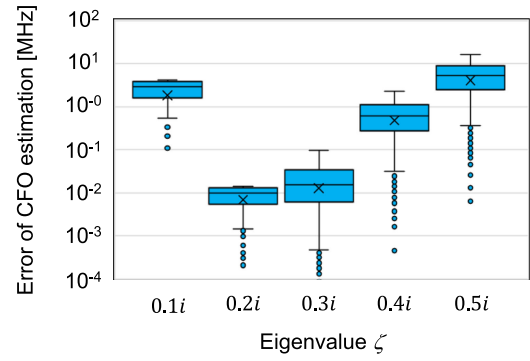


Fig. 9. Box plot of the estimation error without noise.

shift is observed particularly for a large imaginary part $\text{Im}[\zeta]$ and a large frequency shift. As described in Eq. (6), a soliton pulse with an eigenvalue of a large imaginary part such as 0.5 has a high peak and a broad spectrum. In contrast, a soliton pulse with a small imaginary part such as 0.1 requires a large time window size. Therefore, under the condition of limited time window size or bandwidth, the soliton frequency shift represented by the real part of the eigenvalue cannot be exactly detected by IST, which results in the CFO estimation error. In the case of the bandwidth limitation, the maximum error appears at the maximum absolute value of the CFO.

Fig. 9 shows a box plot of the estimation error for a CFO between -2.5 and 2.5 GHz (5 MHz intervals, 1001 samples) on the logarithmic scale. The deviation in the estimation error in the case of W limitation ($0.1i, 0.2i$) is smaller than that in the case of R_s limitation ($0.3i-0.5i$). The circles represent outliers, which are outside 1.5 times the interquartile range above the upper quartile and below the lower quartile. Although there exist lower outliers at the bottom of the period or near a CFO of zero, there are no higher outliers. We consider the maximum estimation error as the worst case for the discussion of the eigenvalue, time window size, and sampling rate dependencies, because it is difficult to adjust the CFO in practical systems.

Second, we discuss the dependence of the estimation error on time window size W and sampling rate R_s . The CFO was estimated from one soliton pulse ($N_p = 1$) for $\text{Re}[\zeta] = 0.25$ under the noiseless condition. Fig. 10(a) and (b) show the maximum value of the estimation error when changing W and R_s , respectively. The maximum estimation error, which was extracted from 1001 CFO values between -2.5 and 2.5 GHz (5 MHz intervals) for each condition, is plotted in Fig. 10. The estimation error decreases with increasing W or R_s . When R_s is fixed, the estimation accuracy is finally limited by R_s even for a large window size, as shown in Fig. 10(a). On the other hand, the minimum estimation accuracy is determined by W for a fixed R_s , as shown in Fig. 10(b). The maximum estimation error can be kept below 10^{-6} MHz ($= 1$ Hz) for $\zeta = 0.25 + 0.1i$, $W = 256, 512$, and $R_s = 1$. When we prepare a sufficiently large W and high R_s , the estimation error approaches zero, and the proposed method provides an unbiased estimation.

Fig. 10(c) shows the maximum estimation error by varying the real part $\text{Re}[\zeta]$ of the eigenvalue for $W = 32$ and $R_s = 1$.

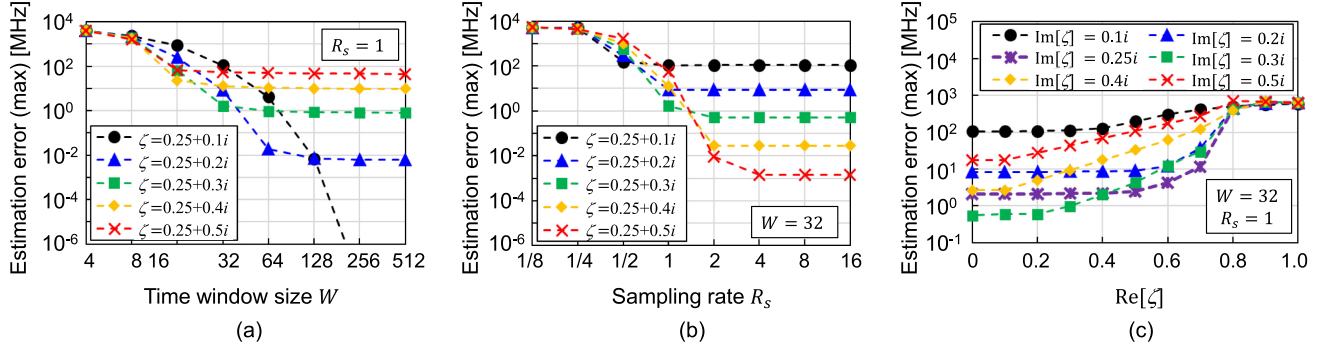


Fig. 10. (a) Time window size dependence ($R_s = 1$), (b) sampling rate dependence ($W = 32$), and (c) $\text{Re}[\zeta]$ dependence ($W = 32$ and $R_s = 1$).

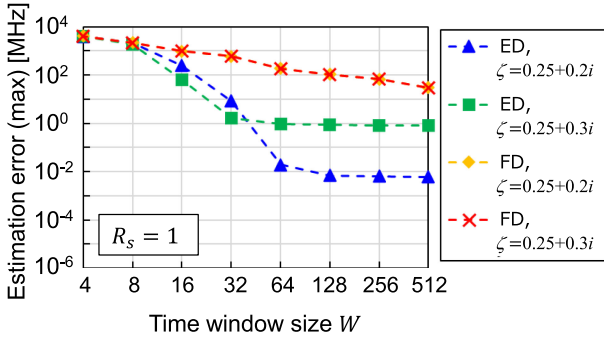


Fig. 11. Comparison with FFT-based method in the FD ($R_s = 1$).

The estimation error increases when the real part is increased. This is because of the eigenvalue shift owing to the bandwidth limitation, as shown in Fig. 8. The estimation accuracy is stable in a range of $\text{Re}[\zeta]$ from 0 to 0.4 for $\text{Im}[\zeta] \leq 0.25$, $W = 32$, and $R_s = 1$.

Fig. 11 shows the maximum estimation errors compared with the FFT-based estimation method in the FD. The estimation error in the FD also decreases with increasing W ; however, it does not change by the imaginary part of eigenvalue $\text{Im}[\zeta]$. The CFO estimation in the ED demonstrates a higher estimation accuracy compared with that in the FD for W from 16 to 512. The CFO estimation in the ED, which detects an eigenvalue as a soliton component, can achieve a fine CFO estimation without additional fittings.

3) Simulation Results With Noise: We investigated the estimation accuracy in the presence of laser phase noise and white Gaussian noise assuming amplified spontaneous emission (ASE) noise. In these simulations with noise, we used the following parameters: $\zeta = 0.25 + 0.25i$, $W = 32$, and $R_s = 1$ assuming an application to an ED-ANN demodulator in the later simulation and experiments.

In the presence of laser phase noise, it induces a deviation of real part of eigenvalue. Fig. 12(a) shows the detected eigenvalue patterns with a phase noise from a laser of the linewidth $\delta f = 1$ MHz for the representative eigenvalue pattern of "0010". We assumed that the phase noise can be modeled as a Wiener process [36]. The eigenvalue deviation owing to laser phase noise is

quite small under the modulation condition of this study even for a wide line width of 1 MHz. Fig. 12(b) and (c) show the variance of the real part of the detected eigenvalue of pattern "0100" with changing linewidth of laser and OSNR, respectively. The phase noise and white Gaussian noise were independently added in Figs. 12(b) and (c). The variation of the real part of the eigenvalue for $\delta f = 1$ MHz was 1.3×10^{-5} , which corresponds to that with white Gaussian noise of OSNR = 22 dB. Therefore, for $\delta f < 1$ MHz, the phase noise effect can be negligible during CFO estimation for an OSNR value considerably lower than 22 dB.

Fig. 13(a) and (b) show the average errors of the CFO estimation with varying numbers of pilot pulses, OSNR, and CFO value. The plotted estimation errors were the average values of 100 sets of the estimation in the CFO range of the target CFO value, ± 12.5 MHz. In the case without noise, the estimation error was 2.2 MHz without relying on the number of pilot pulses, which is determined by the eigenvalue, time window size, and sampling rate, as shown in Fig. 10. With noise loading, the estimation error decreased and asymptotically approached the value without noise by increasing the number of pilot pulses, as shown in Fig. 13(a). The difference in the estimation error among different CFO values was not observed for OSNR = 10 dB, as shown in Fig. 13(b), because the estimation accuracy was limited by the noise in this region. Fig. 13(c) shows a box plot of the estimation error for CFO = 2.5 GHz and OSNR = 10 dB. All estimation errors were maintained below 60 MHz for a CFO of 2.5 GHz when the number of pilot pulses exceeded 2^5 (= 32).

B. Applying to ED-ANN Demodulator

1) Simulation Model: Fig. 14 illustrates the simulation model to investigate the feasibility of the combination of the IST-based CFO compensation and the ED-ANN demodulation.

For eigenvalue modulation, we employed an on-off encoding of four eigenvalues ($N = 4$). The mapping rules between the bit sequences and eigenvalue subsets are summarized in Table II. Although we can select an arbitrary mapping, we followed a typical one-to-one mapping rule of the on-off encoding, where bit "1 (0)" corresponds to "on (off)" state of eigenvalue. We used the following parameters for the eigenvalue-modulated signal at the transmitter: $Z = 8$, a normalized time window width W of

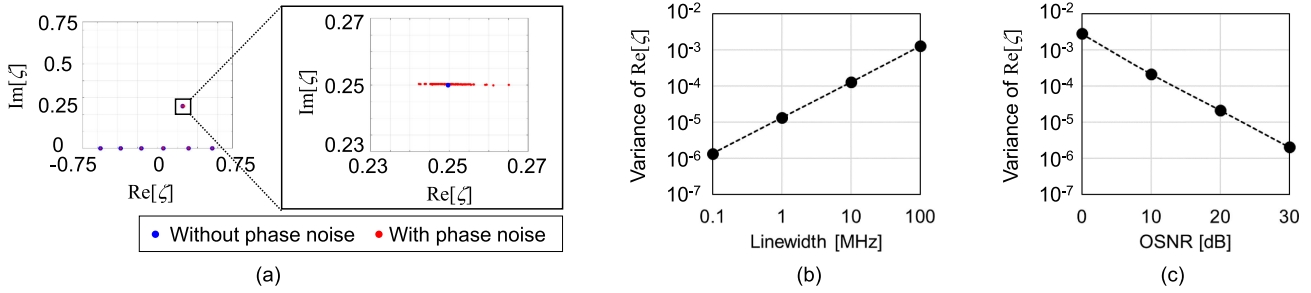


Fig. 12. (a) Detected eigenvalue patterns with a phase noise ($\delta f = 1$ MHz). Variances in the real part of the eigenvalue vs (b) laser linewidth (only phase noise) and (c) OSNR (only white Gaussian noise).

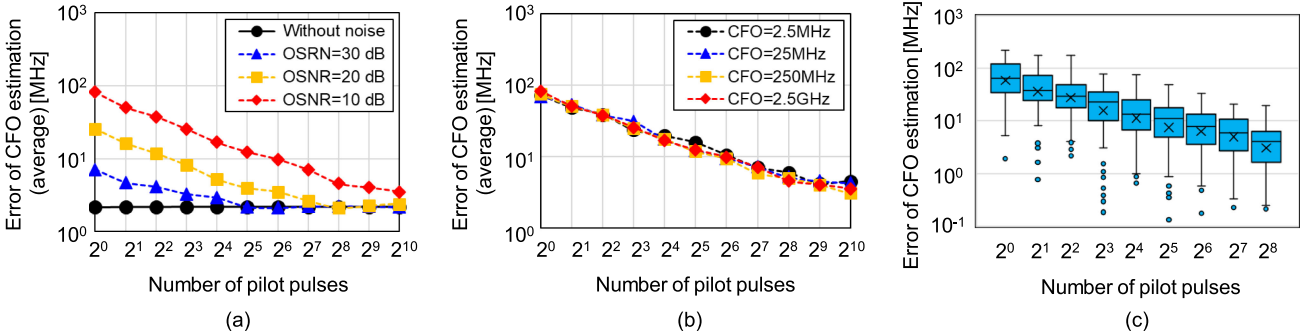


Fig. 13. Errors of CFO estimation: (a) Noise dependence (CFO = 2.5 GHz), (b) CFO dependence (OSNR = 10 dB), (c) box plot of estimation error (CFO = 2.5 GHz, OSNR = 10 dB).

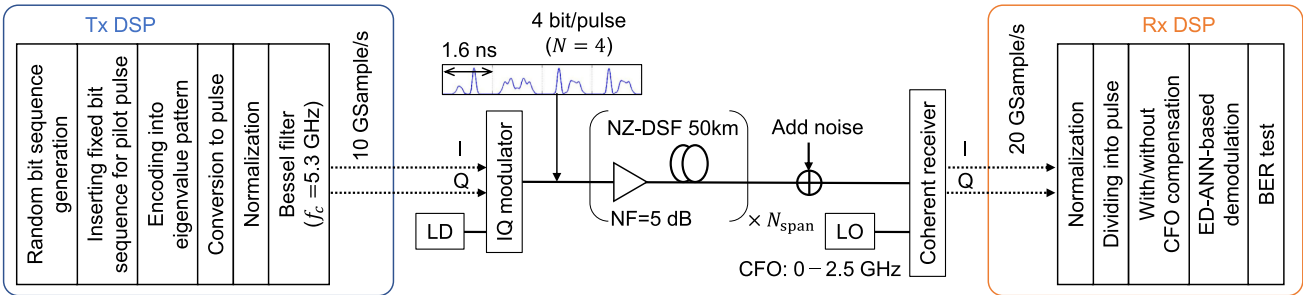


Fig. 14. Simulation model used in this study.

$32 (-16 \leq T \leq 16)$, and $t_0 = 50$ ps. The transmitted signal was pre-dispersed by setting $Z = 8$ to avoid the spectral broadening due to soliton multiplexing around $T = 0$ for $Z = 0$ [32]. Modulation was performed at 10 Gsample/s with a pulse duration of 1.6 ns. Thus, the bit rate was 2.5 Gb/s. First, we confirmed the back-to-back (B-to-B) operation to demonstrate its utility.

At the receiver end, we performed the demodulation with varying CFO values, assuming a difference in frequency between the transmitter laser diode (LD) and receiver LO. We assumed that the laser phase noise was negligible and the CFO was constant in each BER test, except for an investigation of the phase noise effect. White Gaussian noise was added to the eigenvalue-modulated signal in the time domain when evaluating BER. Ideal frequency characteristics were assumed for both the transmitter and receiver, with the exception of Bessel

filtering at the transmitter end. The signal was demodulated using ED-ANN at 20-Gsample/s (32 sample/pulse, $R_s = 1$). The BER was measured in the cases with and without the proposed CFO compensation.

We used the same ED-ANN configuration and parameters for the demodulation as in Section II. A three-layer perceptron configuration and rectified linear unit activation function were considered. The numbers of input, hidden, and output units were set to 64, 256, and 16, respectively. The softmax and cross-entropy error functions were considered as the output and loss functions, respectively. We prepared a block signal that consists of 2,500 pulses of the pilot signal, random pulse sequences of 10,000 for the training, and 50,000 pulses for the validation and BER tests. The block signal length was 100 μ s. The ANN was trained using the Adam optimizer [33] available within the MATLAB R2020a

TABLE II
MAPPING RULES BETWEEN BIT SEQUENCES AND EIGENVALUE SUBSETS

Bit sequence	Eigenvalue subset
0000	None
1000	$0.25 + 0.5i$
0100	$-0.25 + 0.5i$
1100	$0.25 + 0.5i, -0.25 + 0.5i$
0010	$0.25 + 0.25i$
1010	$0.25 + 0.5i, 0.25 + 0.25i$
0110	$-0.25 + 0.5i, 0.25 + 0.25i$
1110	$0.25 + 0.5i, -0.25 + 0.5i, 0.25 + 0.25i$
0001	$-0.25 + 0.25i$
1001	$0.25 + 0.5i, -0.25 + 0.25i$
0101	$-0.25 + 0.5i, -0.25 + 0.25i$
1101	$0.25 + 0.5i, -0.25 + 0.5i, -0.25 + 0.25i$
0011	$0.25 + 0.25i, -0.25 + 0.25i$
1011	$0.25 + 0.5i, 0.25 + 0.25i, -0.25 + 0.25i$
0111	$-0.25 + 0.5i, 0.25 + 0.25i, -0.25 + 0.25i$
1111	$0.25 + 0.5i, -0.25 + 0.5i, 0.25 + 0.25i, -0.25 + 0.25i$

Deep Learning Toolbox. The Adam optimizer was configured using a step size $\alpha = 0.001$, exponential decay rates $\beta_1 = 0.9$ and $\beta_2 = 0.999$, and coefficient $\epsilon = 10^{-8}$. The training data was uniformly extracted from available data sets with CFO=0 Hz and OSNR values in the 0-20 dB range, which obviated the need for re-training for each OSNR level. To avoid over-fitting, the training was terminated when the validation result (obtained once every 50 epochs) stopped improving [34].

For the CFO compensation, we used 32 pilot pulses with an eigenvalue pattern “0010” ($\zeta = 0.25 + i0.25$). The actual pilot pulse rate was 0.064% ($=32 / 50,000$). According to the simulation results shown in Fig. 10(c), we can expect a higher estimation accuracy when using the eigenvalue $0.25 + 0.25i$ than when using $0.25 + 0.5i$, for $W = 32$ and $R_s = 1$. Therefore, we selected the eigenvalue of $0.25 + 0.25i$, which is one of the eigenvalue patterns of the eigenvalue modulated signal, for a simple processing at the receiver.

In addition, we conducted the transmission simulation based on the split-step Fourier method [26] in order to investigate the feasibility to apply the proposed method to long-haul transmission system. The transmission loop consisted of a 50-km non-zero dispersion-shifted fiber (NZ-DSF) and an Er-doped fiber amplifier (EDFA) with a noise figure (NF) of 5 dB. The parameters of the NZ-DSF were as follows: dispersion parameter of 4.4 ps/nm/km, dispersion slope of 0.046 ps/nm²/km, nonlinear coefficient of 2.1 W⁻¹/km, and fiber loss of 0.2 dB/km. The input signal power into the loop was set to -6.3 dBm. The pre-dispersed signal obtained by setting $Z = 8$ was used as the transmitted signal for all the transmission distances.

In our previous work [15], the ED-ANN trained using the training data corresponding to a fixed distance of 3000 km was observed to be perfectly valid for the different transmission distances of over 5000 km in the numerical simulation. In the experiment, we improved the training method because a degradation of the eigenvalue pattern due to the transmission was observed. Eventually, the ED-ANN trained using the mixed training data corresponding to some transmission distances did

not require re-training even when the transmission distance changed in [15]. In the transmission simulation performed in the present study, the ED-ANN was trained using the training data corresponding to CFO = 0 Hz for a fixed transmission distance of 3000 km. Re-training for each CFO, each transmission distance, and each OSNR was not performed. The CFO is compensated using the pilot pulses after the transmission.

2) *Demodulation Results:* Fig. 15(a) and (b) show the BER curves obtained using the test data of various CFOs and the ED-ANN demodulator trained with the training data of CFO = 0 Hz for the B-to-B. In the BER measurements, we assumed that hard-decision FEC was employed with 7% overhead and the FEC limit was 3.8×10^{-3} [35]. Fig. 16 shows the detected eigenvalue patterns with and without the CFO compensation. The eigenvalue patterns are plotted using 100 representative samples with OSNR values of approximately 14 dB. Without the CFO compensation, the ED-ANN is valid for a CFO below 125 MHz with a small power penalty < 1 dB at the FEC limit under the modulation conditions of this simulation. For CFO values over 1 GHz without the CFO compensation, the ED-ANN trained with the data of CFO = 0 Hz cannot demodulate the received signal owing to the large eigenvalue shift, as shown in Fig. 16(a). However, by using the proposed CFO compensation, the eigenvalue shifts were compensated, as shown in Fig. 16(b). Thus, the ED-ANN demodulator with CFO compensation achieved a successful demodulation with insignificant OSNR penalty in the presence of CFO within 2.5 GHz. These results correspond to the CFO estimation accuracy shown in Fig. 13(c), indicating that the remaining CFO effect can be suppressed to less than 60 MHz.

Fig. 15(c) shows the BER curves using the test data after the transmission (CFO = 2.5 GHz) and the ED-ANN demodulator trained with the training data of CFO = 0 Hz for 3000 km. We can confirm successful demodulation with the IST-based CFO compensation even after the transmission. This is because the eigenvalue of the pilot soliton pulse is conserved [15], and the CFO estimation accuracy is limited by the accumulated noise when the appropriate time window size and sampling rate are preserved. However, a small OSNR penalty below 1 dB was observed after the transmission over 4000 km. Fig. 17(a) shows the spectra of the eigenvalue-modulated signal after the transmission with a CFO of 2.5 GHz. The spectra were broadened for 4000 and 5000 km transmission because the pulse shapes and spectra of the multi-soliton pulses change periodically during the transmission. For the CFO of 2.5 GHz and the sampling rate of 20 Gsa/s, the high-frequency components of the eigenvalue-modulated signal were cut off at the receiver. Fig. 17(b) shows the detected eigenvalue patterns with and without the CFO compensation after the transmission (OSNR around 16 dB). We can see that the detected eigenvalue patterns for 4000 and 5000 km were degraded although the eigenvalue shift caused by the CFO was compensated. For example, the pattern “1111” was not symmetrical owing to the spectral distortion. In addition, the eigenvalue deviation became larger due to the spectral broadening. The OSNR penalty was caused by not the CFO estimation error but the above spectral broadening and bandwidth limitation at the receiver.

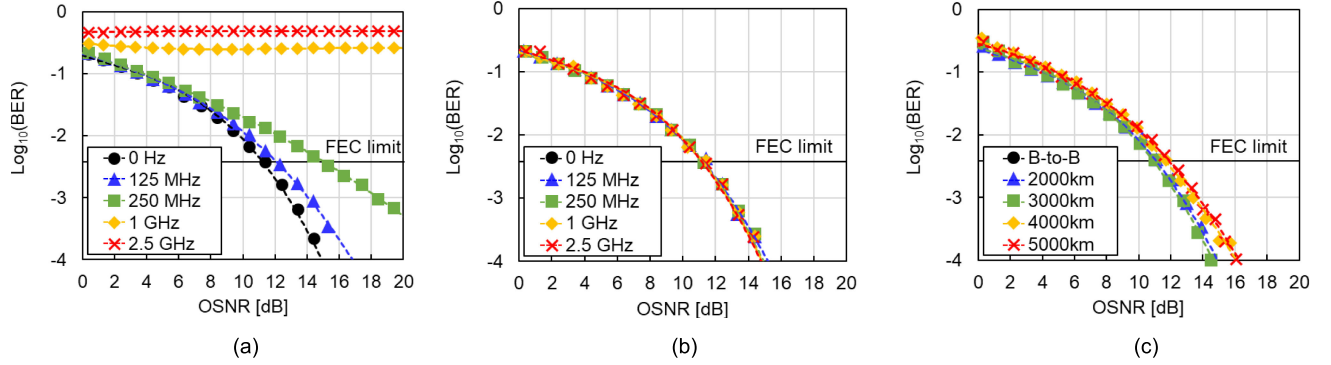


Fig. 15. BER curves obtained by B-to-B simulation (a) without and (b) with the proposed CFO compensation. (c) BER curves obtained by the transmission simulation (CFO = 2.5 GHz).

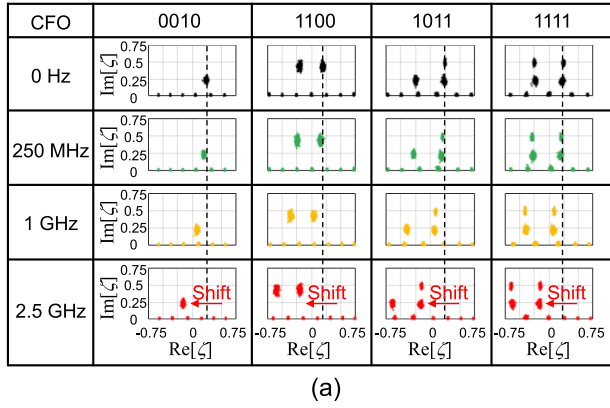


Fig. 16. Representative detected eigenvalue patterns (a) without and (b) with the proposed CFO compensation.

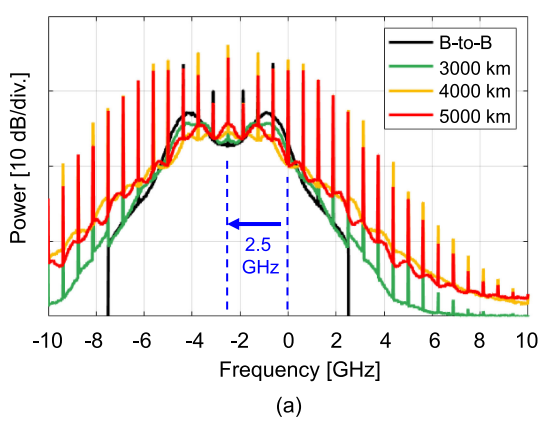


Fig. 17. (a) Spectra of the eigenvalue-modulated signal after the transmission (CFO = 2.5 GHz). (b) Detected eigenvalue patterns with and without the CFO compensation after the transmission (OSNR around 16 dB).

V. EXPERIMENTS

A. Experimental Setup

Fig. 18 depicts an experimental setup for demonstrating the proposed CFO compensation and ED-ANN demodulation. For eigenvalue modulation, the same eigenvalue pattern, comprising

four optical eigenvalues and modulation conditions described in the previous section for the simulation, were considered. An eigenvalue-modulated signal was generated using an offline digital signal processor (DSP). The optical signal was generated using an arbitrary waveform generator (AWG) and an IQ modulator. The ASE noise source before the receiver was

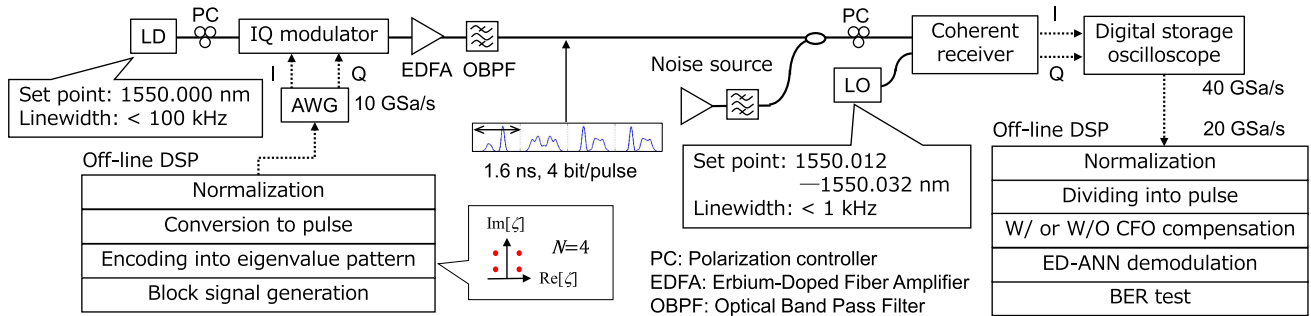


Fig. 18. Experimental setup.

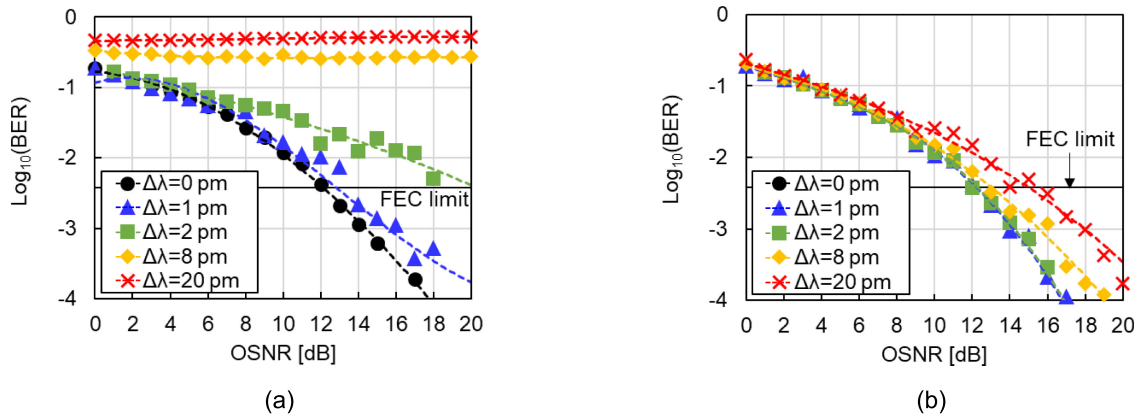


Fig. 19. BER curves obtained by experiment (a) without and (b) with the proposed CFO compensation.

used to measure the BER curves. At the receiver, the required DSP for demodulation was performed offline at 20 Gsample/s. ANN configuration, training condition, and CFO compensation parameters were identically maintained to those described in the simulation. The ED-ANN was trained from scratch using 10,000 eigenvalue patterns obtained from the received training pulses at the fixed CFO in the experiments. We changed the CFO by adjusting the wavelength of the LO light. When the set point of the wavelength λ_{LO} of the LO was 1550.012 nm, the CFO was minimized. Therefore, the ED-ANN was trained for one fixed wavelength of $\lambda_{LO}=1550.012$ nm. The test data were collected in the range of $\lambda_{LO}=1550.012\text{--}1550.032$ nm. In the experiment, the CFO between the training and test signals was estimated and compensated for.

We used the lasers with the linewidths of 100 kHz and 1 kHz for the transmitter and receiver, respectively. In this setup, the maximum and average values of the CFO variation were 500 kHz and 250 kHz for 100 μ s (preamble period) measurement, respectively. The CFO variation was measured by using CW lights and calculating the peak frequency shift for the measurement time T_m , and defined by

$$\text{CFO}_{\text{var}} = \max_t f_{\text{peak}}(t) - \min_t f_{\text{peak}}(t), (0 \leq t \leq T_m). \quad (8)$$

The maximum and average values of CFO_{var} were calculated from the $T_m \times 100$ measurements. For 1 ms measurement, the

maximum and average values of CFO_{var} were 3.2 MHz and 1.4 MHz, respectively.

B. Experimental Results

Fig. 19 depicts the BER curves obtained by varying the set points of wavelengths of LO. $\Delta\lambda$ denotes the difference in wavelength between the training and test data. Without the CFO compensation, an OSNR penalty was maintained less than 1 dB for $\Delta\lambda=1$ pm (~ 125 MHz, equivalent value). However, a large OSNR penalty owing to the eigenvalue shift was observed for $\Delta\lambda$ over 2 pm (~ 250 MHz). Conversely, the ED-ANN with CFO compensation can demodulate an eigenvalue-modulated signal even for $\Delta\lambda=20$ pm (~ 2.5 GHz). However, the OSNR penalties in the experiment were larger than those in the simulation. This is because the vertical shift of the imaginary part of the detected eigenvalue owing to the frequency characteristics of the receiver (reduction in soliton amplitude at high frequency) cannot be compensated perfectly by the IST-based CFO compensation. Fig. 20 depicts the detected eigenvalue patterns of the representative patterns “1011” and “1111” for various $\Delta\lambda$. For a large CFO, such as 2.5 GHz, the vertical eigenvalue shifts remained, although the horizontal eigenvalue shifts were compensated. The OSNR required to achieve the FEC limit of 3.8×10^{-3} is shown in Fig. 21. Using the proposed

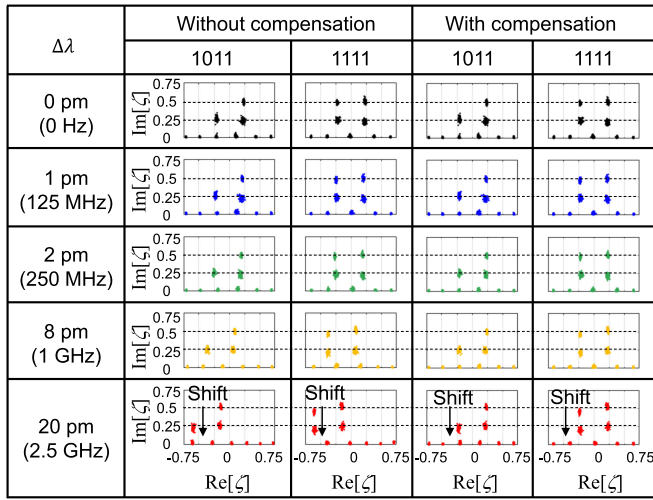


Fig. 20. Detected eigenvalue patterns of the representative patterns “1011” and “1111” for various $\Delta\lambda$.

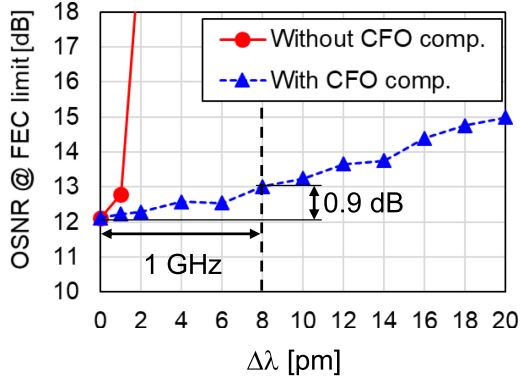


Fig. 21. OSNR required to achieve FEC limit with varying $\Delta\lambda$.

CFO compensation method, the OSNR penalty at the FEC limit can be suppressed below 1 dB when $\Delta\lambda < 8 \text{ pm} (\sim 1 \text{ GHz})$.

Finally, we discuss the pilot pulse rate and frequency stability of the laser. In this experiment, we could suppress the OSNR penalty due to the CFO effect by maintaining the remaining CFO variation for the 1 ms (preamble period) measurement was below 3.2 MHz, the proposed CFO compensation method has the potential to be applicable for lower pilot pulse rates, such as 32 pulses over 625 000 symbols for 1 ms ($\sim 5 \times 10^{-5}$), under the experimental settings used in this study.

VI. CONCLUSION

This study presents an ED-ANN-based demodulation scheme in the presence of optical CFO for eigenvalue-modulated signal. It was found that the conventional ED-ANN demodulator cannot cover an eigenvalue-modulated signal with a large CFO over 1 GHz. To enhance the generalization performance of the ED-ANN on CFO, we proposed to combine an ED-ANN with an IST-based CFO compensation method. The utility of the proposed scheme has been demonstrated via both numerical

simulations and experimental results. Furthermore, the characteristics of the proposed CFO estimation method in the ED, such as dependence of the estimation accuracy on time window size, sampling rate, eigenvalue, and noise effect, were investigated. The proposed method showed a CFO estimation accuracy below 60 MHz for OSNR=10 dB, which contributed to a BER results with no OSNR penalty from CFO effect over 2.5 GHz in the simulation. Furthermore, by performing a proof-of-concept experiment, we successfully demonstrated a demodulation with OSNR penalty $< 1 \text{ dB}$ in the presence of CFO within 1 GHz at 2.5 Gb/s. Thus, the findings of this study reveal the potential of ED-ANN demodulators to cover a large CFO range in the point of generalization performance.

REFERENCES

- [1] A. Hasegawa and T. Nyu, “Eigenvalue communication,” *IEEE/OSA J. Lightw. Technol.*, vol. 11, no. 3, pp. 395–399, Mar. 1993.
- [2] M. J. Ablowitz and H. Segur, *Solitons and the Inverse Scattering Transform*. Philadelphia, PA, USA: SIAM, 1981.
- [3] S. K. Turitsyn *et al.*, “Nonlinear fourier transform for optical data processing and transmission: Advances and perspectives,” *OSA Optica*, vol. 4, no. 3, pp. 307–322, Mar. 2017.
- [4] M. I. Yousefi and F. R. Kschischang, “Information transmission using the nonlinear fourier transform, Part I: Mathematical tools,” *IEEE Trans. Inform. Theory*, vol. 60, no. 7, pp. 4312–4328, Jul. 2014.
- [5] M. I. Yousefi and F. R. Kschischang, “Information transmission using the nonlinear fourier transform, Part II: Numerical methods,” *IEEE Trans. Inform. Theory*, vol. 60, no. 7, pp. 4329–4345, Jul. 2014.
- [6] M. I. Yousefi and F. R. Kschischang, “Information transmission using the nonlinear fourier transform, Part III: Spectrum modulation,” *IEEE Trans. Inform. Theory*, vol. 60, no. 7, pp. 4346–4369, Jul. 2014.
- [7] H. Terauchi and A. Maruta, “Eigenvalue modulated optical transmission system based on digital coherent technology,” in *Proc. 10th Proc. Conf. Lasers Electro-Opt. Pacific Rim, 18th Opto-Electron. Commun. Conf./International Conf. Photon. Switching (CLEO-PR&OECC/PS 2013)*, Kyoto, Japan, 2013, pp. 1–2.
- [8] S. T. Le, V. Aref, and H. Buelow, “Nonlinear signal multiplexing for communication beyond the kerr nonlinearity limit,” *Nature Photon.*, vol. 11, no. 9, pp. 570–577, Sep. 2017.
- [9] T. Gui, T. H. Chan, C. Lu, A. P. T. Lau, and P.-K. A. Wai, “Alternative decoding methods for optical communications based on nonlinear fourier transform,” *IEEE/OSA J. Lightw. Technol.*, vol. 35, no. 9, pp. 1542–1550, May 2017.
- [10] Y. Matsuda, H. Terauchi, and A. Maruta, “Design of eigenvalue multiplexed multi-level modulation optical transmission system,” in *Proc. 19th OptoElectron. Commun. Conf./Australian Conf. on Opt. Fibre Technol. (OECC/ACOFT)*, Melbourne, Australia, Paper Th3C.4, 2014, pp. 1016–1018.
- [11] S. Hari, M. I. Yousefi, and F. R. Kschischang, “Multieigenvalue communication,” *IEEE/OSA J. Lightw. Technol.*, vol. 34, no. 13, pp. 3110–3117, Jul. 2016.
- [12] X. Yangzhang, S. T. Le, V. Aref, H. Buelow, D. Lavery, and P. Bayvel, “Experimental demonstration of dual-polarization NFDM transmission with b-modulation,” *IEEE Photon. Technol. Lett.*, vol. 31, no. 11, pp. 885–888, Jun. 2019.
- [13] K. Mishina, S. Yamamoto, T. Kodama, Y. Yoshida, D. Hisano, and A. Maruta, “Experimental demonstration of neural network based demodulation for on-off encoded eigenvalue modulation,” in *Proc. 45th Eur. Conf. Opt. Commun. (ECOC)*, Dublin, Ireland, Paper W.1.B.4, 2019, pp. 1–4.
- [14] K. Mishina, S. Sato, S. Yamamoto, Y. Yoshida, D. Hisano, and A. Maruta, “Demodulation of eigenvalue modulated signal based on eigenvalue-domain neural network,” in *Proc. Opt. Fiber Commun. Conf.*, San Diego, CA, USA, 2020, Art. no W3D.1.
- [15] K. Mishina, S. Sato, Y. Yoshida, D. Hisano, and A. Maruta, “Eigenvalue-domain neural network demodulator for eigenvalue-modulated signal,” *IEEE/OSA J. Lightw. Technol.*, vol. 39, no. 13, pp. 4307–4317, Jul. 2021.
- [16] R. T. Jones, S. Gaiarin, M. P. Yankov, and D. Ziber, “Time-domain neural network receiver for nonlinear frequency division multiplexed systems,” *IEEE Photon. Technol. Lett.*, vol. 30, no. 12, pp. 1079–1082, Jun. 2018.

- [17] S. Gaiarin, F. Da Ros, N. De Renzis, R. T. Jones, and D. Ziber, "Experimental demonstration of nonlinear frequency division multiplexing transmission with neural network receiver," *IEEE/OSA J. Lightw. Technol.*, vol. 38, no. 23, pp. 6465–6473, Dec. 2020.
- [18] Y. Wu *et al.*, "Robust neural network receiver for multiple-eigenvalue modulated nonlinear frequency division multiplexing system," *OSA Opt. Exp.*, vol. 28, no. 12, pp. 18304–18316, Jun. 2020.
- [19] O. Kotlyar, M. K.-Kopae, M. Pankratova, A. Vasylchenkova, J. E. Prilepsky, and S. K. Turitsyn, "Convolutional long short-term memory neural network equalizer for nonlinear Fourier transform-based optical transmission systems," *OSA Opt. Exp.*, vol. 29, no. 7, pp. 11254–11267, Mar. 2021.
- [20] K. Mishina, D. Hisano, Y. Yoshida, and A. Maruta, "Generalization performance of artificial neural network-based-demodulator for eigenvalue modulated signal," in *Proc. 25th OptoElectron. Commun. Conf.*, Taipei, Taiwan, 2020, Art. no T2-2.2.
- [21] K. Mishina, Y. Yoshida, D. Hisano, and A. Maruta, "Artificial neural network-based-receiver for eigenvalue-modulated signal in presence of optical CFO," in *Proc. 46th Eur. Conf. Opt. Commun., Virtual*, 2020, Art. no We1D-3.
- [22] Optical Internetworking Forum, Integrable Tunable Laser Assembly MSA, (OIF-ITLA-01.2), Jun. 2008.
- [23] Optical Internetworking Forum, Micro Integrable Tunable Laser Assembly (OIF-MicroITLA-01.0), Sep. 2011.
- [24] T. Kodama, T. Zuiki, K. Mishina, and A. Maruta, "Hyper multilevel modulation based on optical eigenvalue multiplexing," in *Proc. Photon. Switching Comput.*, Limassol, Cyprus, 2018, Art. no. Th3C.4.
- [25] A. Hasegawa and Y. Kodama, "Guiding-center soliton in optical fibers," *OSA Opt. Lett.*, vol. 15, no. 24, pp. 1443–1445, Dec. 1990.
- [26] G. P. Agrawal, *Nonlinear Fiber Optics*, 6th ed. Cambridge, MA, USA: Academic Press, 2019.
- [27] A. Maruta, Y. Matsuda, H. Terauchi, and A. Toyota, "Digital coherent technology-based eigenvalue modulated optical fiber transmission system," in *Odyssey of Light in Nonlinear Optical Fibers: Theory and Applications*, K. Porsezian and R. Ganapathy, Ed. Boca Raton, FL, USA: CRC Press, 2015, Chap. 19, pp. 491–505.
- [28] Y. Cao, S. Yu, Y. Chen, Y. Gao, W. Gu, and Y. Ji, "Modified frequency and phase estimation for M-QAM optical coherent detection," in *Proc. 36th Eur. Conf. Opt. Commun.*, Trino, Italy, 2010, Art. no. We.7.A.1.
- [29] M. Selmi, Y. Jaouen, and P. Ciblat, "Accurate digital frequency offset estimator for coherent PolMux QAM transmission systems," in *Proc. 35th Eur. Conf. Opt. Commun.*, Vienna, Austria, 2009, Art. no. P3.08.
- [30] T. Nakagawa *et al.*, "Non-data-aided wide-range frequency offset estimator for QAM optical coherent receivers," in *Proc. Opt. Fiber Commun. Conf.*, Los Angeles, CA, USA, Paper OMJ1, 2011, pp. 1–3.
- [31] Z. Zheng, X. Zhang, R. Yu, L. Xi, and X. Zhang, "Frequency offset estimation for nonlinear frequency division multiplexing with discrete spectrum modulation," *OSA Opt. Exp.*, vol. 27, no. 20, pp. 28223–28238, Sep. 2019.
- [32] K. Mishina, H. Takeuchi, T. Kodama, Y. Yoshida, D. Hisano, and A. Maruta, "4096-ary eigenvalue modulation using 12 triangular-lattice-shaped eigenvalues," in *Proc. Opt. Fiber Commun. Conf., Virtual*, Paper M3I.1, 2021, pp. 1–3.
- [33] D. Kingma and J. Ba, "Adam: A method for stochastic optimization," in *Proc. 3rd Int. Conf. Learn. Representation*, 2015, pp. 1–15.
- [34] I. Goodfellow, Y. Bengio, and A. Courville, *Deep Learning*. Cambridge, MA, USA: MIT Press, 2016.
- [35] ITU-T Recommendation G.975.1, Appendix I.9, Feb. 2004.
- [36] E. Ip and J. M. Kahn, "Feedforward carrier recovery for coherent optical communications," *IEEE/OSA J. Lightw. Technol.*, vol. 25, no. 9, pp. 2675–2692, Sep. 2007.

Ken Mishina (Member, IEEE) received the B.E., M.E., and Ph.D. degrees in electrical, electronic, and information engineering from Osaka University, Osaka, Japan, in 2005, 2007, and 2012, respectively. In 2007, he joined Shimadzu Corporation, Kyoto, Japan. Since 2018, he has been an Associate Professor with the Department of Information and Communication Technology, Division of Electrical, Electronic, and Information Engineering, Graduate School of Engineering, Osaka University. His research interests include optical fiber communication systems, all-optical signal processing, and photovoltaics. He is a Member of IEEE Photonics Society and IEICE, Japan.

Takaya Maeda received the B.E. degree in 2021 in electrical, electronic, and information engineering from Osaka University, Osaka, Japan, where he is currently working toward the M.E. degree.

Daisuke Hisano (Member, IEEE) received the B.E., M.E., and Ph.D. degrees in electrical, electronic, and information engineering from Osaka University, Osaka, Japan, in 2012, 2014, and 2018, respectively. In 2014, he joined NTT Access Network Service Systems Laboratories, Yokosuka, Japan. Since 2018, he has been an Assistant Professor with the Department of Information and Communication Technology, Division of Electrical, Electronic, and Information Engineering, Graduate School of Engineering, Osaka University. His research interests include optical-wireless converged networks, optical communication, and all-optical signal processing. He is a Member of IEICE, Japan.

Yuki Yoshida (Member, IEEE) received the B.S., M.S., and Ph.D. degrees in informatics from Kyoto University, Kyoto, Japan, in 2004, 2006, and 2009, respectively. Between 2009 and 2016, he was an Assistant Professor with Osaka University, Osaka, Japan. Since 2016, he has been a Senior Researcher with the Network Research Institute, National Institute of Information and Communications Technology, Japan. He is also a Visiting Associate Professor with Osaka University. His research interests include digital signal processing for optical/wireless communications, optical/wireless access, and optical-wireless convergence. He is a Member of IEICE, Japan.

Akihiro Maruta (Member, IEEE) received the B.E., M.E., and Ph.D. degrees in communication engineering from Osaka University, Osaka, Japan, in 1988, 1990, and 1993, respectively. In 1993, he joined the Department of Communications Engineering, Osaka University. Since 2016, he has been a Professor with the Department of Information and Communication Technology, Osaka University. His current research interests include optical fiber communication systems and all-optical signal processing. He is a Member of the IEEE Photonics Society and Optical Society of America (OSA), and a Senior Member of IEICE, Japan.